

Fast Kinetic Scheme : efficient MPI parallelization strategy for 3D Boltzmann equation *

Jacek Narski[†]

July 13, 2021

Abstract

In this paper we present a parallelization strategy on distributed memory systems for the Fast Kinetic Scheme — a semi-Lagrangian scheme developed in [J. Comput. Phys., Vol. 255, 2013, pp 680-698] for solving kinetic equations. The original algorithm was proposed for the BGK approximation of the collision kernel. In this work we deal with its extension to the full Boltzmann equation in six dimensions, where the collision operator is resolved by means of fast spectral method. We present close to ideal scalability of the proposed algorithm on tera- and peta-scale systems.

Keywords: Boltzmann equation, kinetic equations, semi-Lagrangian schemes, spectral schemes, 3D/3D, MPI

1 Introduction

Kinetic equations provide a statistical description of non equilibrium particle gases. The evolution of the system is described by a ballistic motion of particles interacting only by a two-body collisions [10, 20]. The Boltzmann model derived originally in 1870s for rarefied gases that are far from thermodynamic equilibrium is nowadays used in variety of applications: ranging from plasma physics to astrophysics, quantum physics, biology and social science. In the Boltzmann description, the state of the system is described by a distribution function defined in seven independent dimensions: the physical space, the velocity space and the time. Moreover, the interaction term requires multiple integrals over velocity space to be evaluated at every space point and for every time step of the numerical method [22, 40]. This makes the kinetic theory very challenging from numerical view point.

There are two major strategies to approach numerically the Boltzmann equation. The first is to apply probabilistic methods such as Direct Simulation Monte Carlo (DSMC) [4, 7, 8, 37]. The second is to choose a deterministic scheme such as finite volume or

*This work was supported by the ANR JCJC project “Moonrise” (ANR-11-MONU-009-01)

[†]Université de Toulouse; UPS, INSA, UT1, UTM; CNRS, UMR 5219; Institut de Mathématiques de Toulouse; F-31062 Toulouse, France. (jacek.narski@math.univ-toulouse.fr)

spectral methods [20, 23, 25, 35, 38]. The probabilistic approach more efficient in terms of computational time. It is however only low order with slow convergence rate.

In this work we choose a semi-Lagrangian approach [11, 12, 23, 24, 32, 42] applied to the transport part of the Boltzmann equation coupled with spectral methods to solve the collision operator [6, 9, 21, 22, 24, 30, 31, 29, 39, 41, 46, 47, 48, 49]. In particular, we consider a Fast Kinetic Scheme (FKS) developed originally for the the Bhatnagar-Gross-Krook (BGK) operator [3] in [13, 14, 17]. The FKS applies the Discrete Velocity Model (DVM) technique, where the velocity space is truncated and discretized with a set of fixed discrete velocities. As a result, the original continuous kinetic equation is replaced by a discrete set of transport equations that can be solved exactly in the semi-Lagrangian framework at practically no cost. In the original method for the BGK operator, where the collisions are modelled as a relaxation towards the local thermodynamic equilibrium, the coupling between equations was included in the computation of the local macroscopic variables (density, momentum, temperature) used to approximate the local equilibrium state. We extend herein the FKS solver to take into account more complex collision models, such as the Boltzmann operator [4, 10]. We make use of the fast spectral method allowing to compute the collision operator in $O(N_v \log N_v)$, where N_v is a number of discrete velocity points in three dimensions [21, 22, 36].

The curse of dimensionality makes numerical simulations of the Boltzmann equation prohibitive on sequential machines even if fast numerical schemes are employed. That is why the need for efficient parallelization strategies arises. The parallel computing in the context of kinetic equations was already explored in [26, 27, 28], where the authors made use of Graphics Processing Unit (GPU) to solve the BGK equation with probabilistic methods. In [34] the authors have implemented the Boltzmann collision kernel on GPU, OpenMP and MPI algorithms were explored in [1, 2, 33, 43, 44]. The FKS parallelization on shared memory systems under OpenMP on GPU was proposed in [15] for the BGK collision kernel. In [16] a simple parallelization strategy on distributed memory systems was proposed for the FKS coupled with Boltzmann collision kernel. The goal of this article is to study in more detail the performance of the FKS on tera- and peta-scale systems. In particular, we propose an efficient hybrid MPI/OpenMP implementation of the scheme with strong scaling close to ideal on available systems.

The article is organized as follows. Section 2 introduces the kinetic equation, the Fast Kinetic Scheme and some collision operators. Section 3 discusses the particle of the FKS interpretation as particularly well suited for parallelization, Section 4 proposes a parallel algorithm and finally Section 5 gives scalability results and some profiling information.

2 Kinetic equations and Fast Kinetic Scheme

In the kinetic theory of rarefied gases, the state of the system is described by a non negative distribution function $f(x, v, t)$. This distribution function describes a density of particles moving with the velocity $v \in \mathbb{R}^3$ at the position $x \in \mathbb{R}^3$ at time t . The evolution of the system is governed by the six dimensional Boltzmann equation

$$\partial_t f + v \cdot \nabla_x f = \mathcal{Q}(f, f), \tag{1}$$

where the operator $\mathcal{Q}(f, f)$ is the collision operator and describes the effect of the collisions on the system. The macroscopic characteristics (density, momentum and energy) are obtained by integrating the distribution function multiplied by 1, v or $|v|^2$ over the velocity space:

$$U = \begin{pmatrix} \rho \\ \rho u \\ E \end{pmatrix} = \int_{\mathbb{R}^3} \phi(v) f dv,$$

where the vector $\phi(v)$ is given by $(1, v, \frac{1}{2}|v|^2)^T$. Typically, the collision operator conserves the macroscopic quantities of the system, *i.e.* the collisions preserve mass, momentum and energy. This is expressed as

$$\int_{\mathbb{R}^3} \phi(v) \mathcal{Q}(f, f) dv = 0$$

and hence the components of the vector $\phi(v)$ are referred to as *collision invariants*.

Multiplying the Boltzmann equation (1) by collision invariants and integrating over the velocity space yields a system of equations for evolution of macroscopic conservative variables

$$\frac{\partial}{\partial t} \int_{\mathbb{R}^3} f \phi(v) dv + \int_{\mathbb{R}^3} v \cdot \nabla_x f \phi(v) dv = 0. \quad (2)$$

This system is not closed as the second term involves higher order moments. However, when the system is at thermal equilibrium, the collision operator $\mathcal{Q}(f, f) = 0$. The equilibrium is characterized by a local Maxwellian distribution

$$M[f] = \frac{\rho}{(2\pi T)^{3/2}} e^{-\frac{(u-v)^2}{2T}},$$

where the temperature T is related to the difference between the total and kinetic energy by the following relation:

$$\frac{3}{2}\rho T = E - \frac{1}{2}\rho|u|^2.$$

Replacing the distribution function f in (2) by the Maxwellian distribution $M[f]$ yields a closed system — a set of Euler equations

$$\begin{aligned} \frac{\partial}{\partial t} \rho + \nabla_x \cdot (\rho u) &= 0, \\ \frac{\partial(\rho u)}{\partial t} + \nabla_x \cdot (\rho u \otimes u + pI) &= 0, \\ \frac{\partial E}{\partial t} + \nabla_x \cdot ((E + p)u) &= 0, \end{aligned}$$

with the pressure following the ideal gas law $p = \rho T$.

The simplest collision operator providing the desired properties (conservation of collision invariant and vanishing at equilibrium) is the Bhatnagar-Gross-Krook operator [3]

$$\mathcal{Q}_{BGK}(f, f) = \nu(M[f] - f),$$

where the inter-particle collisions are modelled as a relaxation process towards local equilibrium. The parameter $\nu = \nu(x, t)$ defines the collision frequency.

The classical Boltzmann collision operator is a multiple integral over the whole velocity space and all possible relative angles:

$$\mathcal{Q}_B(f, f) = \int_{\mathbb{R}^3} \int_{S^2} B(|v - v_\star|, \theta) (f(v')f(v'_\star) - f(v)f(v_\star)) d\omega dv_\star, \quad (3)$$

where v, v_\star are velocities before collision, v', v'_\star the velocities after collision and θ the angle between $v - v_\star$ and $v' - v'_\star$. The post collision velocities are given by

$$v' = \frac{1}{2}(v + v_\star + |v - v_\star|\omega) \quad , \quad v'_\star = \frac{1}{2}(v + v_\star - |v - v_\star|\omega),$$

with ω being a vector on a unitary sphere S^2 . The collision kernel B depends only on the relative velocity before collision and the deflection angle and has the form

$$B(|v - v_\star|, \theta) = |v - v_\star| \sigma(|v - v_\star|, \theta),$$

with σ being the scattering cross section. If the inverse k -th power forces between particles are considered, σ is given by

$$\sigma(|v - v_\star|, \theta) = b_\alpha(\theta) |v - v_\star|^{\alpha-1} \quad (4)$$

with $\alpha = (k - 5)/(k - 1)$. In the framework of the so called *variable hard spheres model* (VHS) $b_\alpha(\theta)$ is constant: $b_\alpha(\theta) = C_\alpha$.

2.1 Fast Kinetic Scheme

Let us now introduce the Fast Kinetic Scheme (FKS) [13, 14] for solving the Boltzmann equation (1). The FKS is a semi-Lagrangian scheme [11, 12, 25] which employs Discrete Velocity Model (DVM) [5, 35] approximation to the original problem.

Let us start by truncating a velocity space. Let us also introduce a cubic grid of N_v equally spaced points in three dimensions. Let us assume for simplicity that the grid step Δv is equal in every direction. Please note however that the FKS is not restricted to Cartesian grids in the velocity space. In fact the method rests unchanged even if unstructured and anisotropic velocity grids are taken into account. Let us now define an approximation of the continuous distribution function $f(x, v, t)$:

$$\tilde{f}_k(x, t) \approx f(x, v_k, t),$$

that is to say, continuous f is replaced by a vector \tilde{f} and the following system of N_v equations is obtained:

$$\partial_t \tilde{f}_k + v_k \cdot \nabla_x \tilde{f}_k = \mathcal{Q}_k(\tilde{f}, \tilde{f}), \quad (5)$$

where $\mathcal{Q}_k(\tilde{f}, \tilde{f})$ is a suitable approximation of the collision operator for the discrete velocity point v_k . This set of equations is coupled only by the collision term.

Let us now discretize the physical space with a Cartesian grid consisting of N_s equally spaced points with a grid step Δx that is equal (for simplicity reasons) in all three directions. Let us also introduce a time discretization with Δt being a time step and $t^n = t^0 + n\Delta t$ for any $n \geq 0$.

In the FKS framework, the equation (5) is solved with a first order splitting technique. First the transport step exactly solves the left hand side of the problem, than the collision step introduces the interaction using the result of the transport step as a starting point:

$$\begin{aligned} \text{Transport stage} &\longrightarrow \partial_t \tilde{f}_k + v_k \cdot \nabla_x \tilde{f}_k = 0, \\ \text{Collisions stage} &\longrightarrow \partial_t \tilde{f}_k = \mathcal{Q}_k(\tilde{f}, \tilde{f}). \end{aligned} \quad (6)$$

Please note that higher order splitting techniques may also be considered.

Transport step

Let $f_{j,k}^n$ be a point-wise approximation of the distribution function at time t^n , position x_j and velocity v_k : $f_{j,k}^n = f(x_j, v_k, t^n)$. The main idea behind FKS is to solve the transport step (6) exactly. Let us define a piece wise constant in space approximation $\bar{f}_k^n(x)$ of the function $\tilde{f}_k(x, t^n)$ such that $\bar{f}_k^n(x) = f(x_j, v_k, t^n)$ if $x \in [x_{j-1/2}, x_{j+1/2}] = \Omega_j$ belongs to the space cell centered on x_j . The exact solution to the transport step at time t^n is therefore given by

$$\bar{f}_k^{*,n+1} = \bar{f}_k^n(x - v_k \Delta t).$$

The function \bar{f}_k^n is advected with a velocity v_k during a time step Δt . The discontinuities of $\bar{f}_k^{*,n+1}$ does coincide now with space cell boundaries after the transport step.

Collision step

During the collision step the amplitude of the distribution function \bar{f} is modified. The collision operator is solved locally on the space grid points and than extended to the whole domain Ω . The following equations (ordinary differential or integro-differential) are solved:

$$\partial_t f_{j,k} = \mathcal{Q}_k(f_{j,\cdot}, f_{j,\cdot}),$$

where $f_{j,k} = f(x_j, v_k, t)$ for all space and velocity grid points $j = 1, \dots, N_s$ and $k = 1, \dots, N_v$ and $f_{j,\cdot}$ is a vector representing the distribution function at the space cell j composed of $f_{j,k}$. The initial data for this equation are provided by the transport step performed before. The time discretization chosen in this work is the first order explicit Euler scheme

$$f_{j,k}^{n+1} = f_{j,k}^{*,n+1} + \Delta t \mathcal{Q}_k(f_{j,\cdot}^{*,n+1}, f_{j,\cdot}^{*,n+1}), \quad (7)$$

where $f_{j,k}^{*,n+1} = \bar{f}_k^{*,n+1}(x_j)$ is the value of transported distribution function at grid point x_j and $f_{j,\cdot}^{*,n+1}$ is a vector composed of $f_{j,k}^{*,n+1}$. Please note that other type of time integrators

can be successfully implemented instead of this forward scheme. In particular the special care must be taken in the stiff limit, please refer to [18, 19].

Equation (7) furnishes a modified value of the distribution function at grid points x_j for velocity points v_k at time t^{n+1} . In order to obtain the value of f at every point of the domain a new piecewise constant function \bar{Q}_k is defined for every discrete velocity v_k :

$$\bar{Q}_k^{n+1}(x) = \mathcal{Q}_k(f_{j,\cdot}^{*,n+1}, f_{j,\cdot}^{*,n+1}) \quad , \quad \forall x \text{ such that } \bar{f}_k^{*,n+1}(x) = f_{j,k}^{*,n+1} \quad ,$$

that is to say, the collision operator at every point of Ω is approximated by a piecewise constant function with discontinuities located at the same points as the piecewise constant function that approximates the distribution function after the transport step. Thanks to this assumption, the spatially reconstructed distribution function after the collision step reads

$$\bar{f}_k^{n+1}(x) = \bar{f}_k^{*,n+1}(x) + \Delta t \bar{Q}_k^{n+1}(x).$$

This completes the description of the Fast Kinetic Scheme.

2.2 Collision operator

Let us now focus on the details related to the collision kernel.

2.2.1 BGK approximation

If particle interaction is modeled by relaxation towards local equilibrium, the collision term $\mathcal{Q}_k(f_{j,\cdot}^{*,n+1}, f_{j,\cdot}^{*,n+1})$ becomes $\nu(\mathcal{E}_{j,k} - f_{j,k})$, where $\mathcal{E}_{j,k}$ is a suitable approximation of the Maxwell distribution for the velocity v_k at the grid point x_j . As the Maxwellian distribution depends on the macroscopic characteristics of the system that are unchanged during the relaxation step (since they are *collision invariants*), the relaxation step (7) becomes completely decoupled. In particular, \mathcal{Q}_k depends only on one velocity point v_k and not on the others.

2.2.2 Boltzmann operator

If the Boltzmann operator is considered, the collision operator $\mathcal{Q}_k(f_{j,\cdot}^{*,n+1}, f_{j,\cdot}^{*,n+1})$ involves integration over whole velocity space for every point x_j of the space grid. The relaxation step is solved by means of Fast Spectral Scheme presented in the Appendix A and requires multiple Fourier transforms to be computed at every time step and at every space cell.

3 Implementation

Let us switch to a particle interpretation of the FKS. Every point of the velocity grid represents a particle moving with velocity v_k . Every space cell Ω_j centered on the space grid point x_j contains exactly the same set of particles at exactly the same relative positions. Therefore one needs to store the particle position and velocity only in one generic cell and not in the whole domain. This reduces the memory requirements seven times:

only mass of the particles is stored for every point of the $6D$ grid, three components of particle position and velocity vectors are only required for the generic reference cell. The distribution function is related to particle masses by

$$f(x, v, t) = \sum_{j,k=1}^{N_s, N_v} \mathbf{m}_{j,k}(t) \delta(x - x_{j,k}(t)) \delta(v - v_{j,k}(t)), \quad v_{j,k}(t) = v_k,$$

where $x_{j,k}(t)$ is particle position, $v_{j,k}(t)$ is its velocity and $\mathbf{m}_{j,k}(t)$ particle mass. In the FKS the particle velocity is unchanged and the position is altered during the transport step:

$$x_{j,k}(t + \Delta t) = x_{j,k}(t) + v_{j,k}(t) \Delta t.$$

The transport step moves the particles in the reference cell. The motion of particles in the remaining cells is identical. If a given particle escapes the generic cell, another one with the same velocity (but different mass) enters the cell from the opposite side.

The collision step modifies the particle masses in every space cell:

$$\mathbf{m}_{j,k}(t + \Delta t) = \mathbf{m}_{j,k}(t) + \Delta t Q_k(v_{j,\cdot}),$$

where $Q_k(v_{j,\cdot})$ is the approximation of the collision operator in the center of the cell by the means of the fast spectral method presented above.

The macroscopic variables at time t^n are defined on the space grid only and are computed as a sum over particles in the given cell j :

$$U_j^n = \sum_{k=0}^{N_v} \phi(v_{j,k}) \mathbf{m}_{j,k}^n (\Delta v)^3.$$

As the collision step does not change the macroscopic conservative variables, they can be efficiently computed at time t^{n+1} after the transport step by adding the contribution from the particles leaving and entering the given cell j to the values at the previous time step. If a particle (j, k) is transported to the cell $j + \delta$ during the transport step, there is a sister particle entering the cell j from $j - \delta$. A suitable contribution has to be added to from the conservative variables in the cell j :

$$U_j^{n+1} = U_j^n + \sum_{k, x_{j,k}^{n+1} \in \Omega_{j+\delta}, x_{j,k}^n \in \Omega_j} (\mathbf{m}_{j-\delta,k}^n - \mathbf{m}_{j,k}^n) \phi(v_{j,k}) (\Delta v)^3 \quad (8)$$

The most expensive part in the algorithm is the collision operator. Even in the case of the relatively simple BGK approximation the computation of the relaxation term takes 90% of the computational time on serial machines [15]. The cost of the Boltzmann integral is substantially greater, even if the Fast Spectral Method is employed. Indeed, a number of FFTs must be performed for every space cell and for every discrete angle in order to compute convolutions. If 16 discrete angles are considered ($A_1 = A_2 = 4$), this number equals 96 and even if the size of those transforms is relatively small, this represents the

main computational burden. Evaluation of the Boltzmann operator represents more than 99% of the computational time on serial machines. Fortunately the collision operator is in some sense decoupled from the FKS framework: it can be implemented independently of the FKS. This suggests a following strategy for the parallelization on distributed memory systems. On the upper level, the FKS is parallelized with MPI over available computational nodes. On the collision level, a suitable operator is implemented on the available node architecture: using the classical OpenMP type parallelism or the SIMD (Single Instruction, Multiple Data) programming model on GPUs or on the Intel Many Integrated Core (MIC) hardware. The implementation details of the collision operator does not influence the MPI scalability of the algorithm.

4 Fast Kinetic Scheme on parallel machines

In this section we propose a simple parallelization strategy for distributed memory systems. There are two possible approaches: the first one is to decompose velocity space and distribute it over computational nodes keeping all spatial degrees of freedom at every node. This approach is very similar to the strategy employed in the GPU algorithm for the BGK collision kernel (*cf.* [15]), where for each velocity point from the velocity mesh a relaxation term was computed in parallel for all space cells at once on a GPU device. It was also chosen in [43] for the MPI implementation. Every computational node performs computations of a relaxation for a subset of velocity grid. Then the partial moments are evaluated. The total moments are obtained from gathering all contributions from all computational nodes. This approach is well suited for collision kernels that are local, *e.g.* for the BGK approximation, where the collision computed for a given position in physical and velocity space depends only on the distribution function at the same position and on total moments. As every node contains all spatial degrees of freedom, no particle escapes given computational node and no particle mass is exchanged with neighbouring nodes. The MPI communication is limited only to the partial moments. Another advantage is that even if a complicated domain is considered *i.e.* containing perforations, no complicated domain decomposition or load balancing techniques are required to ensure equal workloads across computational nodes. However, any collision kernel that is non-local would generate huge amount of communication between all processors. Boltzmann collision operator involve a double integral over velocity space meaning that at every iteration every node must have access to the whole velocity space. This approach is therefore not well suited for the Boltzmann operator.

The second possibility, adopted herein, is to distribute spatial degrees of freedom over computational nodes, keeping on every node a complete velocity space. Since the update of conservative variables (density, momentum and energy) requires an exchange of particle mass with neighbouring spatial cells (and does not involve any summation over whole physical space), the internodal memory transfer is limited to merely cells located on a boundary of a subdomain. Moreover, the information is exchanged with one node only and not with every node reserved for the computation. Comparison of the two approaches can be found in [44].

The spatial domain is decomposed into equally sized non-overlapping cuboids, pencils or slabs with ghost layers. Depending on the choice, every node has to communicate with 2 (for slabs), 8 (for pencils) or 26 (for cuboids) neighboring nodes. Cuboids usually minimize the size of ghost layers but have the biggest MPI overhead as they require more calls to MPI in order to communicate with all neighbors. Thus, the cuboid domain decomposition strategy is not necessarily optimal and better results can be sometimes obtained when using pencils or slabs.

Moreover, the performance of the method can be improved by OpenMP or SIMD parallelization applied to the loops over velocity space at each node. This kind of parallelization for shared memory systems was already proposed in [15]. Let us now, for the sake of completeness, repeat the sequential and parallel algorithms for shared memory systems.

4.1 Sequential algorithms for FKS

We consider particle positions \mathbf{X}_p^n and masses $m_{j,p}^n$ known at time t^n as well as conservative F_j^n and primitives variables $(\rho, \mathbf{U}, T)_j^n$. The algorithm reads:

1. *Transport of particles.* Displace N_v particles with (6), produce a list of N_{out} particles escaping the generic cell and store the δ s determining the destination and provenance of associated sister particles.
2. *Update conservative variables* U_j^{n+1} using (8) and the results from the transport step.
3. *Relaxation step.* Compute masses of N_v particles with a collision kernel of choice, store them in an array of the size $N_v \times N_s$.

4.2 Classical parallel architecture: Open-MP

The modified algorithm reads:

1. *Relaxation step.* Divide the number of spatial cells by the number of processors. Compute in parallel the masses of N_v particles with a collision kernel of choice, parallelization is performed on the loop over the number of mesh points in the physical space. This computation is local on the space mesh.
2. *Transport of particles.* Move in parallel N_v particles with (6). This step is done in only one space cell. The motion of particles in the other cells is the same.
3. *Update conservative variables.* Test in a parallel loop over the number of mesh points in the physical space if a particle has escaped from the generic cell. If so, add a contribution to U_j^{n+1} using (8) for every space cell. Update the particle position and exchange particle mass with the associated sister particle.

4.3 Graphic Processing Unit (GPU) architecture: CUDA

This parallelization design can be summarized in the following algorithm.

1. *Copy from CPU to GPU.* Copy to the GPU memory all primitive and conservative variables.
2. *Loop over N_v particles*
 - (a) *Relaxation step* Compute relaxed masses of particles for every space cell using CUDA. Store the result on GPU.
 - (b) *Transport step* Move every N_v particle and test if it has escaped the generic cell. If so, store the provenance cell of the sister particle.
 - (c) *Update conservative variables.* If the particle has escaped the generic cell, add contribution to conservative variables. Reassign its mass and position with the ones of the incoming sister particle.
 - (d) *Copy from GPU to CPU.* Copy the resulting mass array from the GPU memory to the CPU memory.
3. *Copy from GPU to CPU.* Write to the CPU memory the updated conservative and primitive variables.

4.4 MPI version of FKS

The parallel algorithm is straightforward

1. *Initialization* Divide the computational domain into $N_{MPI} = N_{MPI_x} \times N_{MPI_y} \times N_{MPI_z}$ equally sized cuboids. Allocate memory on each computational node: arrays of the size N_s/N_{MPI} for storing the conservative and primitive variables relative to a given subdomain and an array of the size $N_v \times (N_s/N_{MPI} + N_{ghosts})$ for storing masses relative to a given subdomain with additional ghost layers containing masses of particles in the adjacent space cells.
2. *Time iterations* For every computational node:
 - (a) *Relaxation step* performed in parallel on GPU or with OpenMP for every particle in a given subdomain.
 - (b) *Transport of particles.* Move in parallel N_v particles with (6). This step is done in only one space cell in each subdomain. The motion of particles in the other cells is the same.
 - (c) *Communication* If a particle is escaping from a given subdomain, broadcast its mass to suitable computational node.
 - (d) *Update conservative variables.* If the particle has escaped the generic cell, add contribution to conservative variables. Reassign its mass and position with the ones of the incoming sister particle. For particles located on the boundary of

the cuboid and escaping the subdomain use the values stored in the ghost cells in the previous step.

3. *Finalization* Free memory and close MPI communication.

The communication is limited only to neighboring subdomains. The amount of data to be exchanged depends only on the local mesh size and chosen MPI topology (slabs / pencils / cuboids). It does not depend on number of computational nodes employed. Weak scaling is therefore evident.

5 Performance tests

Numerical tests for the BGK collision kernel were performed on the EOS supercomputer at CALMIP, Toulouse. The supercomputer is equipped with 612 computational nodes, each of them containing two Intel[®] Ivy Bridge 2.8GHz 10 core CPUs and 64 GB of RAM. Each CPU was equipped with 25MB of cache memory. The code was compiled with gcc-5.3.0 and executed on 2 to 90 computational nodes. That is to say, on 40 to 1800 computational cores in parallel. The tests for Boltzmann collision kernel were performed on the EOS supercomputer ($N = 64^3$ meshes) and on the thin nodes of GENCI-TGCC supercomputer Curie for $N = 128^3$. The machine is equipped with 5040 B510 Bullx nodes (called thin nodes), each containing two Intel[®] Sandy Bridge 2.7GHz 8 core CPUs (20MB of cache memory) and 64GB of RAM. In the case of the Boltzmann collision operator the Fast Fourier Transforms were computed by means of the fftw library, version 3.3.4. The code was executed with 20 OpenMP threads per node on EOS and 16 OpenMP threads per node on Curie.

The performance of the parallel algorithm was tested on the 3D Sod test case. The problem description is a 3D explosion problem [45], the initial state being given by the well known Sod shock tube problem. Let us consider a cubic domain of size $[0, 2]^3$. Left and right states of the 1D Sod problem are given by a density $\rho_L = 1$, mean velocity $\mathbf{U}_L = \mathbf{0}$ and temperature $\theta_L = 5$, while $\rho_R = 0.125$, $\mathbf{U}_R = \mathbf{0}$, $\theta_R = 4$. The gas is initially in thermodynamic equilibrium. The left state is set for any cell inside a ball centered in $(1, 1, 1)$ and of radius 0.2. The right state is set elsewhere. The computations are stopped at final time $t_{\text{final}} = 0.07$ for the BGK operator and after 16 iterations for the Boltzmann operator. This number of time steps ensured that every discrete particle has changed the physical cell at least once. We consider the case in which $\tau = 10^{-1}$, *i.e.* far from the fluid limit. We are not interested in the convergence of the numerical solution but in the parallel efficiency only. Some convergence results and more interesting (from physical point of view) test cases are presented in [16].

The performance tests were run for the BGK and 3D Boltzmann collision kernels. Computation of the 3D Boltzmann collision operator is much more time consuming compared to the BGK operator. The run time is 100 times bigger for $N_v = 32^3$ velocity points. The ratio increases even more for larger velocity meshes. We expect that all the communication time and MPI overhead will be hidden for the 3D Boltzmann operator with MPI efficiency close to one on the supercomputer at our disposal. When dealing

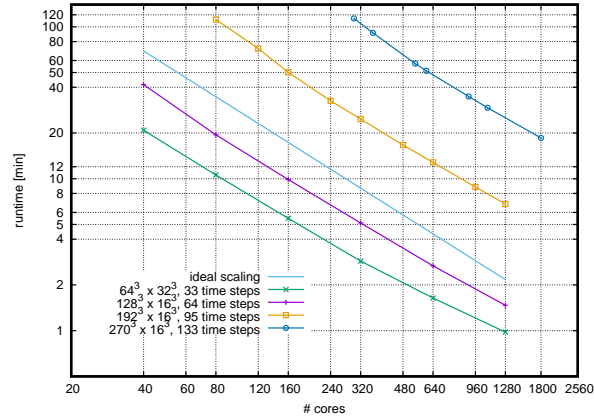


Figure 1: Computational time as a function of number of cores employed for BGK.

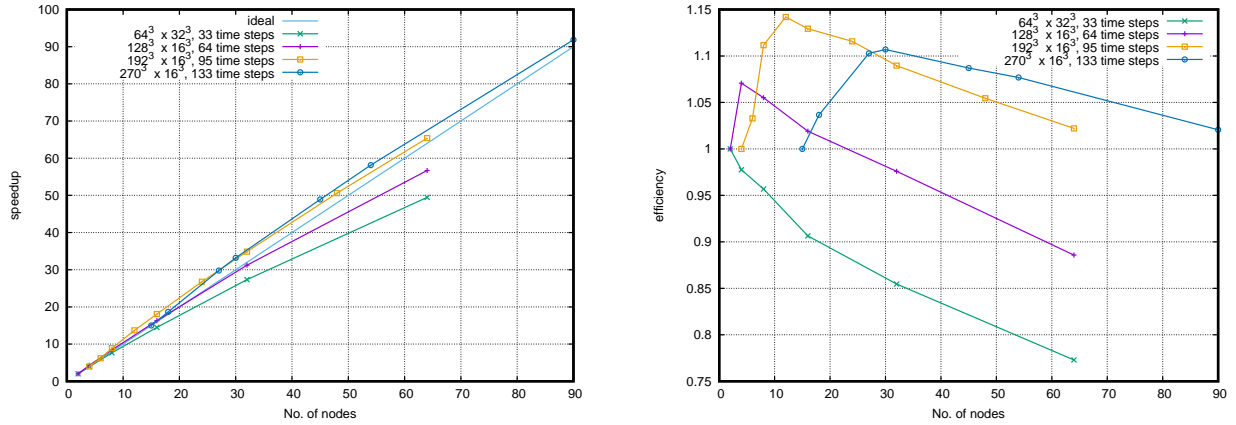


Figure 2: Speedup (left) and efficiency (right) as a function of number of computational nodes for BGK. A minimal number of nodes requisite to run the test is equal to 2 for $64^3 \times 32^3$ and $128^3 \times 16^3$ mesh and to 4 for the $192^3 \times 16^3$ mesh.

with the BGK kernel it is the memory requirement that is a real bottleneck. Indeed, BGK $3D \times 3D$ simulations on medium size meshes can be efficiently performed on multi-core or GPU based shared memory systems with enough RAM at disposition with runtime that of the order of hours or days rather than weeks or months [15]. However, if fine scale simulations are required the MPI parallelization is indispensable.

5.1 BGK

Let us first discuss numerical results for the BGK collision kernel. Simulations were run on four different meshes:

- $N = 64^3$ and $N_v = 32^3$,
- $N = 128^3$ and $N_v = 16^3$,
- $N = 192^3$ and $N_v = 16^3$.
- $N = 270^3$ and $N_v = 16^3$.

The memory required for storage of the mass array was equal to 64Gb in the first two cases, to 216Gb in the third case and to 600Gb in the last case. The minimal number of computational nodes required to run the Sod test case was therefore equal to 2 for the first two cases, to 4 in the third case and to 15 in the last case.

Let us first compare different domain decomposition strategies for the first mesh ($N = 62^3$ and $N_v = 32^3$) to find the optimal one. The computations were run on $N_{MPI} = 2, 4, 8, 16, 32$ and 64 nodes. The domain was decomposed into slabs, pencils or cuboids. The elapsed run time is shown in Table 1. For $N_{MPI} = 4$ nodes the best results are obtained for the computational domain divided into 4 slabs. This coincides with the smallest number of the ghost cells. For 8 nodes the shortest run time is still obtained for the slab configuration, even though the number of ghost cells is 28% bigger than for the pencil configuration. The run time for the latter is only slightly bigger. The cuboid type domain decomposition gives the biggest run time. For 16 nodes the run time for slab and pencil like decomposition is very close to each other with relative difference of the order of 1%. We note that the best performance was obtained for a pencil like decomposition with $N_{MPI_x} = 8$ and $N_{MPI_y} = 2$. For 32 and 64 nodes the best performance was obtained again for pencil like decomposition. The cuboid type decomposition resulted in a run time comparable with the slab configuration and from 7% to 12% bigger than the run time for the best configuration despite the fact that the number of ghost cells was the smallest (almost 5 time smaller than the number of ghost cells for slab configuration on 64 nodes). The weak performance of the cuboid configuration is due to a greater MPI overhead caused by communication with significantly bigger number of nodes.

The scalability test were performed with the optimal domain decomposition strategy. The run time as a function of computational cores is presented on the Figure 1 and the speedup with parallel efficiency (relative to the smallest number of nodes employed in the test) on the Figure 2. For the second mesh the scaling is almost perfect with some super-linear behaviour when passing from 2 to 4 computational nodes and some loss of performance when going from 32 to 64 for nodes. For the smallest mesh there is no super-linearity observed, the performance loss is observed when passing from 16 to 32 and then to 64 computational nodes. For the third and fourth mesh the super-linearity appears between 4 and 16 nodes employed, parallel efficiency is above 0.95 for 2–32 nodes. The scaling for the last mesh seems to be super linear in the whole tested range with parallel efficiency above one. This super linear scaling is probably due to the CPU cache

N_{MPI}	N_{MPI_x}	N_{MPI_y}	N_{MPI_z}	time	#neigh.	#cells	#ghosts
2	2	1	1	1376.51	2	131072	8192
4	4	1	1	704.064	2	65536	8192
	2	2	1	712.356	8	65536	8448
8	8	1	1	359.652	2	32768	8192
	4	2	1	362.894	8	32768	6400
	2	2	2	386.392	26	32768	6536
16	16	1	1	191.856	2	16384	8192
	8	2	1	189.828	8	16384	5376
	4	4	1	191.113	8	16384	4352
	4	2	2	201.823	26	16384	4424
32	32	1	1	106.414	2	8192	8192
	16	2	1	101.946	8	8192	4864
	8	4	1	100.669	8	8192	3328
	8	2	2	106.942	26	8192	3368
	4	4	2	108.903	26	8192	2824
64	64	1	1	63.5180	2	4096	8192
	32	2	1	58.7658	8	4096	4608
	16	4	1	55.6507	8	4096	2816
	16	2	2	59.4585	26	4096	2840
	8	8	1	56.5515	8	4096	2304
	8	4	2	59.3814	26	4096	2024
	4	4	4	62.6682	26	4096	1736

Table 1: Computational time, number of neighboring nodes, number of data cells per node and number of ghost cells per node as a function of MPI size (N_{MPI}) and domain decomposition (MPI dimensions N_{MPI_x} , N_{MPI_y} , N_{MPI_z}) for the BGK kernel test case on the $64^3 \times 32^3$ mesh. The smallest number of ghost cells and the smallest run time are written in bold type for every tested MPI size N_{MPI} .

performance. For all four mesh sizes there is a linear decrease in parallel efficiency for growing number of nodes.

Tables 2–5 show the total run time T , time spent on a single cycle $T_{\text{cycle}} = T/N_{\text{cycle}}$, average time spent on a single cell per cycle $T_{\text{cell}} = T_{\text{cycle}}/N_c$ and finally the average time spent by a single node on a single cell per cycle $T_{\text{cell/node}} = N_{MPI}T_{\text{cycle}}$ for different number of nodes employed. The performance loss is observed when the subdomain size become relatively small. This is manifested in the increase of the average time per cycle spent by one node on a single cell. This is due to the fact that the internodal communication time becomes comparable with the time spent on computations.

The size of spatial mesh allocated in every node seems also to influence the cache performance at the nodes. On Tables 2, 3 and 4 the non linear scaling is observed for small number of nodes — the average time per cell per cycle per node is decreasing when the number of nodes increases. The best performance is observed on 30 nodes for the 270^3 mesh ($656 \cdot 10^3$ cells per node), on 12 nodes for 192^3 mesh ($590 \cdot 10^3$ cells per node) and on 4 nodes on 128^3 mesh ($524 \cdot 10^3$ cells per node).

N_V	Vel.	Cell #	#nodes	N_{cycle}	Time(s)	T_{cycle}	T_{cell}	$T_{\text{cell/node}}$
16^3	[-15, 15]	$270^3 \times 16^3$ $= 80.6 \times 10^9$	15 (300 cores)	133	6815.39	51.2	$2.60 \cdot 10^{-6}$	$3.91 \cdot 10^{-5}$
			18 (360 cores)		5479.12	41.2	$2.09 \cdot 10^{-6}$	$3.77 \cdot 10^{-5}$
			27 (540 cores)		3433.45	25.8	$1.31 \cdot 10^{-6}$	$3.54 \cdot 10^{-5}$
			30 (600 cores)		3078.33	23.1	$1.18 \cdot 10^{-6}$	$3.53 \cdot 10^{-5}$
			45 (900 cores)		2089.94	15.7	$7.98 \cdot 10^{-7}$	$3.59 \cdot 10^{-5}$
			54 (1080 cores)		1758	13.2	$6.72 \cdot 10^{-7}$	$3.63 \cdot 10^{-5}$
90 (1800 cores)	1112.93	8.37	$4.25 \cdot 10^{-7}$	$3.83 \cdot 10^{-5}$				

Table 2: Performance tests on $270^3 \times 16^3$ mesh for BGK. Time per cycle is obtained by $T_{\text{cycle}} = T/N_{\text{cycle}}$, time per cycle per cell by $T_{\text{cell}} = T_{\text{cycle}}/N_c$ and time per cycle per node by $T_{\text{cycle/node}} = N_s T_{\text{cell}}$.

N_V	Vel.	Cell #	#nodes	N_{cycle}	Time(s)	T_{cycle}	T_{cell}	$T_{\text{cycle/node}}$
16^3	[-15, 15]	$192^3 \times 16^3$ $= 29 \times 10^9$	4 (80 cores)	95	6696.82	70.5	$9.96 \cdot 10^{-6}$	$3.98 \cdot 10^{-5}$
			6 (120 cores)		4322.4	45.5	$6.43 \cdot 10^{-6}$	$3.86 \cdot 10^{-5}$
			8 (160 cores)		3012.17	31.7	$4.48 \cdot 10^{-6}$	$3.58 \cdot 10^{-5}$
			12 (240 cores)		1954.71	20.6	$2.91 \cdot 10^{-6}$	$3.49 \cdot 10^{-5}$
			16 (320 cores)		1482.56	15.6	$2.20 \cdot 10^{-6}$	$3.53 \cdot 10^{-5}$
			24 (480 cores)		1000.37	10.5	$1.49 \cdot 10^{-6}$	$3.57 \cdot 10^{-5}$
			32 (640 cores)		768.273	8.09	$1.14 \cdot 10^{-6}$	$3.66 \cdot 10^{-5}$
			48 (960 cores)		529.223	5.57	$7.87 \cdot 10^{-7}$	$3.78 \cdot 10^{-5}$
64 (1280 cores)	409.52	4.31	$6.09 \cdot 10^{-7}$	$3.90 \cdot 10^{-5}$				

Table 3: Performance tests on $192^3 \times 16^3$ mesh for BGK. Time per cycle is obtained by $T_{\text{cycle}} = T/N_{\text{cycle}}$, time per cycle per cell by $T_{\text{cell}} = T_{\text{cycle}}/N_c$ and time per cycle per node by $T_{\text{cycle/node}} = N_s T_{\text{cell}}$.

N_V	Vel.	Cell #	#nodes	N_{cycle}	Time(s)	T_{cycle}	T_{cell}	$T_{\text{cell/node}}$
16^3	[-15, 15]	$128^3 \times 16^3$ $= 8.6 \times 10^9$	2 (40 cores)	64	2499.49	39.1	$1.86 \cdot 10^{-5}$	$3.72 \cdot 10^{-5}$
			4 (80 cores)		1167.2	18.2	$8.70 \cdot 10^{-6}$	$3.48 \cdot 10^{-5}$
			8 (160 cores)		592.256	9.25	$4.41 \cdot 10^{-6}$	$3.53 \cdot 10^{-5}$
			16 (320 cores)		306.597	4.79	$2.28 \cdot 10^{-6}$	$3.65 \cdot 10^{-5}$
			32 (640 cores)		160.077	2.50	$1.19 \cdot 10^{-6}$	$3.82 \cdot 10^{-5}$
64 (1280 cores)	88.1792	1.38	$6.57 \cdot 10^{-7}$	$4.20 \cdot 10^{-5}$				

Table 4: Performance tests on $128^3 \times 16^3$ mesh for BGK. Time per cycle is obtained by $T_{\text{cycle}} = T/N_{\text{cycle}}$, time per cycle per cell by $T_{\text{cell}} = T_{\text{cycle}}/N_c$ and time per cycle per node by $T_{\text{cycle/node}} = N_s T_{\text{cell}}$.

N_V	Vel.	Cell #	#nodes	N_{cycle}	Time(s)	T_{cycle}	T_{cell}	$T_{\text{cell/node}}$
32^3	[-15, 15]	$64^3 \times 32^3$ $= 8.6 \times 10^9$	2 (40 cores)	33	1250.51	37.9	$1.45 \cdot 10^{-4}$	$2.89 \cdot 10^{-4}$
			4 (80 cores)		635.297	19.3	$7.34 \cdot 10^{-5}$	$2.94 \cdot 10^{-4}$
			8 (160 cores)		328.987	9.97	$3.80 \cdot 10^{-5}$	$3.04 \cdot 10^{-4}$
			16 (320 cores)		172.168	5.22	$1.99 \cdot 10^{-5}$	$3.18 \cdot 10^{-4}$
			32 (640 cores)		98.2927	2.98	$1.14 \cdot 10^{-5}$	$3.64 \cdot 10^{-4}$
		64 (1280 cores)		58.6773	1.78	$6.78 \cdot 10^{-6}$	$4.34 \cdot 10^{-4}$	

Table 5: Performance tests on $64^3 \times 32^3$ mesh for BGK. Time per cycle is obtained by $T_{\text{cycle}} = T/N_{\text{cycle}}$, time per cycle per cell by $T_{\text{cell}} = T_{\text{cycle}}/N_c$ and time per cycle per node by $T_{\text{cycle/node}} = N_s T_{\text{cell}}$.

There is no such effect observed on Table 5. Let us now compare Tables 4 and 5. The dimension of the problem is the same. In the first case the domain was discretized with 128^3 points in the physical space and with the 16^3 velocity points. In the second case a spatial mesh of the size 64^3 was used and a velocity mesh of the size 32^3 , giving a total of $8.6 \cdot 10^9$ degrees of freedom. The size of the spatial mesh per node is eight times smaller in second case while the number of degrees of freedom is the same in both cases. The $N = 128^3$ mesh seems to perform better than the 64^3 one with time per cycle being smaller and with better MPI efficiency. This is not surprising as the amount of data exchanged with neighbouring nodes is at least 2 times smaller.

Table 6 shows profiling data for the $64^3 \times 32^3$ mesh on 2 and 64 nodes as well as for the $270^3 \times 16^3$ mesh on 90 computational nodes. For the coarse mesh the time spent on the BGK collision operator decreases from 65% (on 2 nodes) to 50% (on 64 nodes) while on the fine mesh the relaxation term takes more than 70% of the computational time (on 90 nodes). This explains the efficiency loss for larger number of nodes: the time spent on the BGK operator is too small to hide internodal communication. Please note that better parallelization strategy can be applied for this collision model: decomposition of the velocity space (instead of physical) would require less data exchange between MPI processes in this particular case and yield therefore a better parallel efficiency. This alternative approach is however not suited for the Boltzmann collision operator.

5.2 3D Boltzmann

Let us now turn our attention to the 3D Boltzmann collision kernel. This task is much more demanding in terms of computational time as the relaxation routine involves multiple and expensive calls to the Fast Fourier Transform. The tests were run on following meshes:

- $N = 64^3$ and $N_v = 16^3$,
- $N = 64^3$ and $N_v = 32^3$.
- $N = 128^3$ and $N_v = 32^3$.

	Cycle	CPU (s)	Main routines	Cost CPU vs total (s)	Cost vs total (%)
$64^3 \times 32^3$ 2 nodes	32	1374	Transport	0.0028	$2 \cdot 10^{-4}\%$
			ToConservative	269.123	19.59%
			ToPrimitive	0.01	$7 \cdot 10^{-4}\%$
			Collision	904.166	65.8%
			Communication	200.718	14.61%
			=	1374.02	100%
$64^3 \times 32^3$ 64 nodes	32	56	Transport	0.0027	$4.9 \cdot 10^{-3}\%$
			ToConservative	18.06	32.34%
			ToPrimitive	0.0008	$1.4 \cdot 10^{-3}\%$
			Collision	28.113	50.34%
			Communication	9.67	17.31%
			=	55.85	100%
$270^3 \times 16^3$ 90 nodes	133	1038	Transport	0.0041	$4 \cdot 10^{-4}\%$
			ToConservative	234.78	22.62%
			ToPrimitive	0.053	$5 \cdot 10^{-3}\%$
			Collision	751.36	72.4%
			Communication	51.59	4.97%
			=	1037.76	100%

Table 6: Profiling of the average cost for each routine for the BGK collision operator on $64^3 \times 32^3$ mesh for 32 time steps and for $270^3 \times 16^3$ mesh for 133 time steps.

The tests for the $N = 64^3$ meshes were performed on slab type domain decomposition. The results are presented on Figures 3 and 4 and on Tables 7 and 8. For the last mesh computations were performed for 16 time steps and until the final time $t_f = 0.07$ was reached. This clearly does not allow to present any physically interesting results but is enough to study the parallel efficiency of the herein proposed method as during this time every particle will change a space cell at least once. The tests were run on N_{MPI} ranging from 16 to 1024. That is to say on 128 to 2048 processors and on 1024 to 16384 computational cores. The results are presented on Table 9 and on Figures 3 and 4.

A comparison of the run times obtained for the second mesh (see Figure 3) with the run time obtained for the BGK collision kernel shows that the latter is approximately 100 times faster. As the time spent on the computation of the relaxation kernel is now much more important, the communication time becomes negligible even if the size of the subdomains is small. The method shows the strong scaling that is close to ideal for all tested meshes with no efficiency loss observed (see Figure 4) and the parallel efficiency close to one. Also, the average time spent by one computational node on one cell per cycle does not depend on number of nodes employed in the computations. The method clearly enjoys the strong scaling close to ideal in the tested range.

Comparison of the run time for both meshes shows that multiplying the number of Fourier modes by 2 in each direction results in a run time multiplied by 16 instead of 8. This loss of performance is related to the computational complexity of the fast spectral solver for the Boltzmann collision kernel which is of $O(N_v \log N_v)$ as well as to the cache

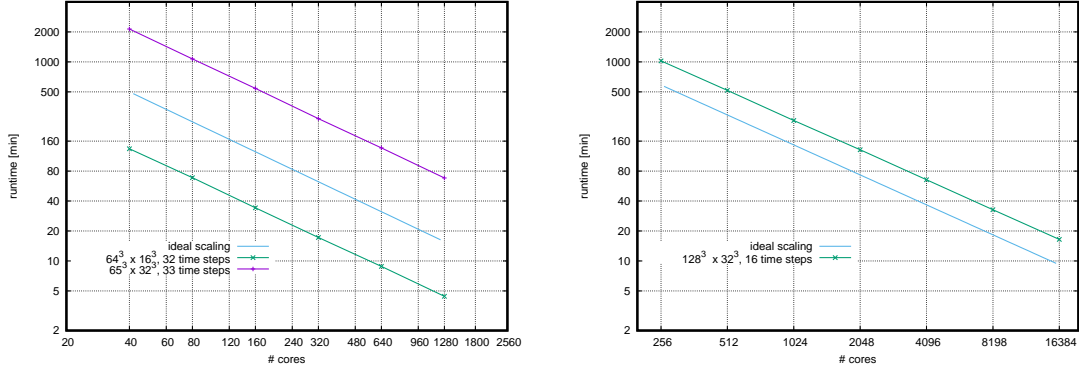


Figure 3: Computational time as a function of number of cores employed on EOS machine (left panel) and on TGCC-CURIE (right panel).

performance. Each CPU performs 10 (8 on Curie) FFTs in parallel at the same time. The size of one transform required for the convolution computation is 32^3 for the 16^3 Fourier modes. This means that the memory required to store 10 vectors containing 32^3 complex values in double precision format for 10 in-place transforms is 5MB, which is less than the cache capacity. For the finer mesh the memory required is 40MB, that is to say four times more than the cache of the CPU.

N_V	Vel.	Cell #	#nodes	N_{cycle}	Time(s)	T_{cycle}	T_{cell}	$T_{\text{cell/node}}$
16^3	[-15, 15]	$64^3 \times 16^3$ $= 1.07 \times 10^9$	2 (40 cores)	33	8043.07	244	$9.3 \cdot 10^{-4}$	$1.86 \cdot 10^{-3}$
			4 (80 cores)		4119.41	125	$4.76 \cdot 10^{-4}$	$1.90 \cdot 10^{-3}$
			8 (160 cores)		2053.01	62.2	$2.37 \cdot 10^{-4}$	$1.90 \cdot 10^{-3}$
			16 (320 cores)		1031.67	31.3	$1.19 \cdot 10^{-4}$	$1.91 \cdot 10^{-3}$
			32 (640 cores)		529.246	16	$6.12 \cdot 10^{-5}$	$1.96 \cdot 10^{-3}$
			64 (1280 cores)		264.725	8.02	$3.06 \cdot 10^{-5}$	$1.96 \cdot 10^{-3}$

Table 7: Performance tests on $64^3 \times 16^3$ mesh for Boltzmann collision kernel. Time per cycle is obtained by $T_{\text{cycle}} = T/N_{\text{cycle}}$, time per cycle per cell by $T_{\text{cell}} = T_{\text{cycle}}/N_c$ and time per cycle per node by $T_{\text{cycle/node}} = N_s T_{\text{cell}}$.

Table 10 shows the profiling data for 16 and 1024 computational nodes. Time spent on MPI communication increases from 1.23% to 3.75%. Collision step takes above 95% of the total run time and hides the parallelization costs.

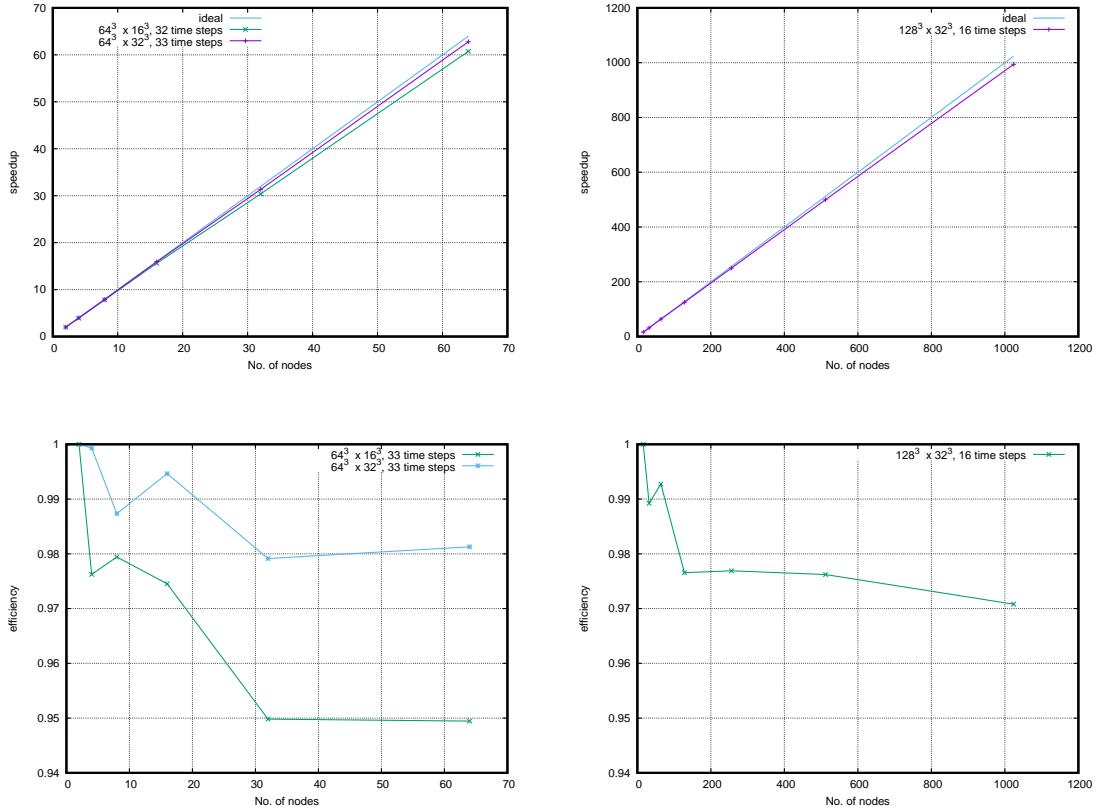


Figure 4: Speedup (top) and efficiency (bottom) as a function of number of computational nodes for 3D Boltzmann collision kernel on EOS machine (left panel) and on TGCC-CURIE (right panel).

6 Conclusions

In this paper we have presented an extension of the Fast Kinetic Scheme introduced in [13] to the Boltzmann collision operator by means of Fast Spectral Method and possible MPI parallelization. The obtained strong scaling is closed to ideal in the tested range (up to 1024 computational nodes) for $3D \times 3D$ problems for the Boltzmann operator. In the proposed method the physical space was distributed over computational nodes by means of the MPI. Each node was supplied with a complete velocity grid. This approach has proven to be well suited for velocity non local collision operators (like Boltzmann) and performs less good for simplified and velocity local models (BGK). The reason is that the BGK collision kernel is much less resource demanding — computational time spent on particle interaction in one space cell is two orders of magnitude smaller compared to the full Boltzmann operator. Better performance for the BGK operator could be obtained by employing the following alternative: distribute velocity space over computational nodes

N_V	Vel.	Cell #	#nodes	N_{cycle}	Time(s)	T_{cycle}	T_{cell}	$T_{\text{cell/node}}$
32^3	[-15, 15]	$64^3 \times 32^3$ $= 8.6 \times 10^9$	2 (40 cores)	33	128378	3890	$1.48 \cdot 10^{-2}$	$2.97 \cdot 10^{-2}$
			4 (80 cores)		64233.2	1950	$7.43 \cdot 10^{-3}$	$2.97 \cdot 10^{-2}$
			8 (160 cores)		32506.4	985	$3.76 \cdot 10^{-3}$	$3.01 \cdot 10^{-2}$
			16 (320 cores)		16133.7	489	$1.87 \cdot 10^{-3}$	$2.98 \cdot 10^{-2}$
			32 (640 cores)		8194.58	248	$9.47 \cdot 10^{-4}$	$3.03 \cdot 10^{-2}$
			64 (1280 cores)		4088.34	124	$4.73 \cdot 10^{-4}$	$3.02 \cdot 10^{-2}$

Table 8: Performance tests on $64^3 \times 32^3$ mesh for Boltzmann collision kernel. Time per cycle is obtained by $T_{\text{cycle}} = T/N_{\text{cycle}}$, time per cycle per cell by $T_{\text{cell}} = T_{\text{cycle}}/N_c$ and time per cycle per node by $T_{\text{cycle/node}} = N_s T_{\text{cell}}$.

N_V	Vel.	Cell #	#nodes	N_{cycle}	Time(s)	T_{cycle}	T_{cell}	$T_{\text{cell/node}}$
32^3	[-15, 15]	$128^3 \times 32^3$ $= 69 \times 10^9$	16 (256 cores)	16	61346.4	3834.2	$1.83 \cdot 10^{-3}$	$2.93 \cdot 10^{-2}$
			32 (512 cores)		31006.9	1937.9	$9.24 \cdot 10^{-4}$	$2.96 \cdot 10^{-2}$
			64 (1024 cores)		15448.8	965.6	$4.60 \cdot 10^{-4}$	$2.95 \cdot 10^{-2}$
			128 (2048 cores)		7852.4	490.8	$2.34 \cdot 10^{-4}$	$3.00 \cdot 10^{-2}$
			256 (4096 cores)		3924.8	245.3	$1.17 \cdot 10^{-4}$	$2.99 \cdot 10^{-2}$
			512 (8192 cores)		1963.7	122.7	$5.85 \cdot 10^{-5}$	$3.00 \cdot 10^{-2}$
1024 (16384 cores)	987.37	61.71	$2.94 \cdot 10^{-5}$	$3.01 \cdot 10^{-2}$				

Table 9: Performance tests on $128^3 \times 32^3$ mesh for Boltzmann collision kernel for 16 time steps. Time per cycle is obtained by $T_{\text{cycle}} = T/N_{\text{cycle}}$, time per cycle per cell by $T_{\text{cell}} = T_{\text{cycle}}/N_c$ and time per cycle per node by $T_{\text{cycle/node}} = N_s T_{\text{cell}}$.

and supply every node with a complete physical space. This approach would minimize the communication for the BGK kernel. However, the optimal algorithm for this operator is not the scope of this paper and numerical results were presented only to illustrate the computational complexity of the Boltzmann operator. The algorithm was tested on classical architectures with collision kernels parallelized locally by the means of OpenMP. We expect to maintain the similar scaling on GPU or Intel MIC based node architectures, which is the scope of future works.

Acknowledgements

This work has been supported by the french 'Agence Nationale pour la Recherche (ANR)' in the frame of the contract "Moonrise" (ANR-11-MONU-009-01). Numerical simulations were performed using HPC resources from GENCI-TGCC (Grant 2016-AP010610045) and from CALMIP (project P1542). The author would like to acknowledge fruitful discussions with G.Dimarco, F.Filbet and R.Loubère.

	Cycle	CPU (s)	Main routines	Cost CPU vs total (s)	Cost vs total (%)
16 nodes	16	61346	Transport	0.0032	5 10 ⁻⁶ %
			ToConservative	175.2	0.29%
			ToPrimitive	0.0056	9 10 ⁻⁶ %
			Collision	60418.6	98.5%
			Communication	752.59	1.23%
			=	61346.4	100%
1024 nodes	16	987	Transport	0.0043	4.3 10 ⁻³ %
			ToConservative	6.16	0.62%
			ToPrimitive	0.00028	2.9 10 ⁻⁶ %
			Collision	944.222	95.63%
			Communication	36.98	3.75%
			=	987.365	100%

Table 10: Profiling of the average cost for each routine for the Boltzmann collision kernel on $128^3 \times 32^3$ mesh for 16 time steps.

A Boltzmann collision operator

The Boltzmann collision operator is solved by the means of Fast Spectral Scheme presented in this section for a selected time step t^n and a selected grid point x_j . The same computation is repeated for other grid points and time steps. In this section we denote by f the distribution function (of v only) at time t^n and point x_j : $f = f(v) = f(x_j, v, t^n)$.

In order to compute the Boltzmann integral (3), let us suppose that the distribution function f has a compact support on the ball $B_0(R)$ of radius R centered in the origin. It can be shown [39, 40] that the support of the collision operator $Q(f, f)$ is included in the ball $B_0(\sqrt{2}R)$ and

$$Q_B(f, f) = \int_{B_0(2R)} \int_{S^2} B(|g|, \theta) (f(v')f(v'_1) - f(v)f(v-g)) d\omega dg$$

with $v', v'_1, v-g \in B_0((2+\sqrt{2})R)$. We can therefore restrict f to the cube $[-T, T]^3$ with $T \geq (2+\sqrt{2})R$ assuming $f(v) = 0$ on $[-T, T]^3 \setminus B_0(R)$ and then extend it to a periodic function on $[-T, T]^3$. As a consequence of the periodicity of f it is sufficient to take $T \geq (3+\sqrt{2})R/2$ to prevent overlapping of the regions where f is different from zero [40]. In order to simplify notation let us take $T = \pi$ and $R = \lambda\pi$ with $\lambda = 2/(3+\sqrt{2})$. Let $Q_B^R(f)$ denote the Boltzmann operator with cut-off. Let us perform a discrete Fourier transform on f obtaining

$$f_N(v) = \sum_{k=-N/2}^{N/2} \hat{f}_k e^{ik \cdot v},$$

$$\hat{f}_k = \frac{1}{(2\pi)^3} \int_{[-\pi, \pi]^3} f(v) e^{-ik \cdot v} dv.$$

with k being a multi-index $k = (k_x, k_y, k_z)$ and $N = (\sqrt[3]{N_v}, \sqrt[3]{N_v}, \sqrt[3]{N_v})$ is vector containing the number of velocity discretization points (Fourier modes) in each direction. Let us impose that the residue of the collision step is orthogonal to any trigonometric polynomial of degree less or equal than N in order to obtain a set of ODEs for coefficients \hat{f}_k :

$$\int_{[-\pi, \pi]^3} \left(\frac{\partial f_N}{\partial t} - \mathcal{Q}_B^R(f_N) \right) e^{-ik \cdot v} dv = 0.$$

After some computation we obtain

$$\hat{Q}_k := \int_{[-\pi, \pi]^3} \mathcal{Q}_B^R(f_N) e^{-ik \cdot v} dv = \sum_{\substack{l, m = -N/2 \\ l+m=k}}^{N/2} \hat{f}_l \hat{f}_m \hat{\beta}(l, m), \quad k = -N, \dots, N, \quad (9)$$

where $\hat{\beta}(l, m) = \hat{B}(l, m) - \hat{B}(m, m)$ are given by

$$\hat{B}(l, m) = \int_{B_0(2\lambda\pi)} \int_{S^2} |q| \sigma(|q|, \cos \theta) e^{-i(l \cdot q^+ + m \cdot q^-)} d\omega dq.$$

with

$$q^+ = \frac{1}{2}(q + |q|\omega), \quad q^- = \frac{1}{2}(q - |q|\omega).$$

Finally, the set of ODEs is obtained:

$$\frac{\partial \hat{f}_k}{\partial t} = \sum_{\substack{l, m = -N/2 \\ l+m=k}}^{N/2} \hat{\beta}(l, m) \hat{f}_l \hat{f}_m$$

supplied with the initial condition

$$\hat{f}_k(0) = \frac{1}{(2\pi)^3} \int_{[-\pi, \pi]^3} f_0(v) e^{-ik \cdot v} dv.$$

Straightforward evaluation of (9) is expensive, especially in three dimensions, the cost being of the order of $O(N^2)$. In order to reduce the computational cost the so called Carleman representation of (3) is used:

$$\mathcal{Q}_B(f, f) = \int_{\mathbb{R}^3} \int_{\mathbb{R}^3} \tilde{B}(x, y) \delta(x \cdot y) [f(v+y) f(v+x) - f(v+x+y) f(v)] dx dy,$$

with

$$\tilde{B}(|x|, |y|) = 2^2 \sigma \left(\sqrt{|x|^2 + |y|^2}, \frac{|x|}{\sqrt{|x|^2 + |y|^2}} \right) (|x|^2 + |y|^2)^{-\frac{1}{2}}.$$

Under the k -th power inter particle force assumption (4) this becomes

$$\tilde{B}(|x|, |y|) = 4C_\alpha (|x|^2 + |y|^2)^{-\frac{1-\alpha}{2}}. \quad (10)$$

The new quadrature formula is obtained:

$$\hat{Q}_k = \sum_{\substack{l, m = -N/2 \\ l+m=k}}^{N/2} \hat{\beta}_F(l, m) \hat{f}_l \hat{f}_m, \quad k = -N, \dots, N$$

where $\hat{\beta}_F(l, m) = \hat{B}_F(l, m) - \hat{B}_F(m, m)$ are now given by

$$\hat{B}_F(l, m) = \int_{B_0(R)} \int_{B_0(R)} \tilde{B}(x, y) \delta(x \cdot y) e^{i(l \cdot x + m \cdot y)} dx dy.$$

The next step is to identify a convolution structure. The goal is to approximate $\hat{\beta}_F(l, m)$ by a sum

$$\hat{\beta}_F(l, m) \simeq \sum_{p=1}^A \alpha_p(l) \alpha'_p(m),$$

where A represents a finite number of possible collision directions. This is a discrete sum of A convolutions and as a consequence the computational cost of the algorithm is of the order of $O(AN \log N)$.

This convolution can be obtained under assumption that $\tilde{B}(|x|, |y|)$ is separable:

$$\tilde{B}(|x|, |y|) = a(|x|)b(|y|).$$

This is the case if α is set to one in (10): $\tilde{B}(|x|, |y|) = 4C_\alpha$. In particular, when $\tilde{B}(|x|, |y|) = 1$, this corresponds to the hard spheres model. In this framework the following quadrature formula for $\hat{B}_F(l, m)$ is obtained:

$$\hat{B}_F(l, m) = \frac{\pi^2}{A_1 A_2} \sum_{p, q=0}^{A_1, A_2} \alpha_{p, q}(l) \alpha'_{p, q}(m),$$

where

$$\begin{aligned} \alpha_{p, q}(l) &= \phi_R^3(l \cdot e_{(\theta_p, \varphi_q)}), & \alpha'_{p, q}(m) &= \psi_R^3\left(\Pi_{e_{(\theta_p, \varphi_q)}^\perp}(m)\right), \\ \phi_R^3(s) &= \int_{-R}^R \rho e^{i\rho s} d\rho, & \psi_R^3(s) &= \int_0^\pi \sin \theta \phi_R^3(s \cos \theta) d\theta, \end{aligned}$$

and the discrete angles θ_p and φ_q are defined by

$$(\theta_p, \varphi_q) = \left(\frac{p\pi}{A_1}, \frac{q\pi}{A_2}\right).$$

References

- [1] V. V. Aristov and S. A. Zabelok. A deterministic method for solving the Boltzmann equation with parallel computations. *Comput. Math. Math. Phys.*, 42(3):425–437, 2002.
- [2] C. Baranger, J. Claudel, N. Hérouard, and L. Mieussens. Locally refined discrete velocity grids for stationary rarefied flow simulations. *Journal of Computational Physics*, 257, Part A:572 – 593, 2014.
- [3] P. L. Bhatnagar, E. P. Gross, and M. Krook. A model for collision processes in gases. I. Small amplitude processes in charged and neutral one-component systems. *Phys. Rev.*, 94(3):511–525, 1954.
- [4] G. A. Bird. *Molecular gas dynamics and the direct simulation of gas flows*. Oxford University Press, 2nd edition, 1994.
- [5] A. V. Bobylev, A. Palczewski, and J. Schneider. On approximation of the Boltzmann equation by discrete velocity models. *C. R. Acad. Sci. Paris Ser. I Math.*, 320(5):639–644, 1995.
- [6] A. V. Bobylev and S. Rjasanow. Difference scheme for the Boltzmann equation based on the fast Fourier transform. *Eur. J. Mech. B Fluids*, 16(2):293–306, 1997.
- [7] R. E. Caflisch. Monte carlo and quasi-monte carlo methods. *Acta numerica*, 7:1–49, 1998.
- [8] R. E. Caflisch and L. Pareschi. Towards a hybrid Monte Carlo method for rarefied gas dynamics. In *Transport in Transition Regimes*, pages 57–73. Springer, 2004.
- [9] C. Canuto, M. Hussaini, A. Quarteroni, and T. A. Zang. *Spectral methods in fluid dynamics*. Springer Series in Computational Physics. Springer-Verlag, New York, 1988.
- [10] C. Cercignani. *The Boltzmann equation and its applications*, volume 67 of *Applied Mathematical Sciences*. Springer-Verlag, New York, 1988.
- [11] N. Crouseilles, M. Mehrenberger, and E. Sonnendrücker. Conservative semi-Lagrangian schemes for Vlasov equations. *Journal of Computational Physics*, 229(6):1927–1953, 2010.
- [12] N. Crouseilles, T. Respaud, and E. Sonnendrücker. A forward semi-lagrangian method for the numerical solution of the vlasov equation. *Computer Physics Communications*, 180(10):1730–1745, 2009.
- [13] G. Dimarco and R. Loubère. Towards an ultra efficient kinetic scheme. Part I: Basics on the BGK equation. *Journal of Computational Physics*, 255:680–698, 2013.

- [14] G. Dimarco and R. Loubère. Towards an ultra efficient kinetic scheme. Part II: The high order case. *Journal of Computational Physics*, 255:699–719, 2013.
- [15] G. Dimarco, R. Loubère, and J. Narski. Towards an ultra efficient kinetic scheme. Part III: High-performance-computing. *Journal of Computational Physics*, 284:22–39, 2015.
- [16] G. Dimarco, R. Loubère, J. Narski, and T. Rey. An efficient numerical method for solving the boltzmann equation in multidimensions. *Submitted, arXiv:1608.08009*, 2016.
- [17] G. Dimarco, R. Loubère, and V. Rispoli. A multiscale fast semi-Lagrangian method for rarefied gas dynamics. *Journal of Computational Physics*, 291:99–119, 2015.
- [18] G. Dimarco and L. Pareschi. High order asymptotic-preserving schemes for the Boltzmann equation. *C. R. Math. Acad. Sci. Paris*, 350(9-10):481–486, 2012.
- [19] G. Dimarco and L. Pareschi. Asymptotic preserving implicit-explicit Runge-Kutta methods for nonlinear kinetic equations. *SIAM J. Numer. Anal.*, 51(2):1064–1087, 2013.
- [20] G. Dimarco and L. Pareschi. Numerical methods for kinetic equations. *Acta Numer.*, 23:369–520, 2014.
- [21] F. Filbet and C. Mouhot. Analysis of spectral methods for the homogeneous Boltzmann Equation. *Trans. Amer. Math. Soc.*, 363:1947–1980, 2011.
- [22] F. Filbet, C. Mouhot, and L. Pareschi. Solving the Boltzmann equation in $N \log^2 N$. *SIAM J. Sci. Comput.*, 28(3):1029–1053, 2007.
- [23] F. Filbet and G. Russo. High order numerical methods for the space non-homogeneous Boltzmann equation. *J. Comput. Phys.*, 186(2):457–480, Apr. 2003.
- [24] F. Filbet and G. Russo. Accurate numerical methods for the Boltzmann equation. In *Modeling and computational methods for kinetic equations*, pages 117–145. Springer, 2004.
- [25] F. Filbet, E. Sonnendrücker, and P. Bertrand. Conservative numerical schemes for the Vlasov equation. *J. Comput. Phys.*, 172(1):166–187, Sept. 2001.
- [26] A. Frezzotti, G. P. Ghiroldi, and L. Gibelli. Direct solution of the boltzmann equation for a binary mixture on gpus. *AIP Conference Proceedings*, 1333(1):884–889, 2011.
- [27] A. Frezzotti, G. P. Ghiroldi, and L. Gibelli. Solving model kinetic equations on GPUs. *Comput. & Fluids*, 50:136–146, 2011.
- [28] A. Frezzotti, G. P. Ghiroldi, and L. Gibelli. Solving the Boltzmann equation on GPUs. *Comput. Phys. Comm.*, 182(12):2445–2453, 2011.

- [29] I. M. Gamba and J. R. Haack. A conservative spectral method for the Boltzmann equation with anisotropic scattering and the grazing collisions limit. *J. Comput. Phys.*, 270:40–57, 2014.
- [30] I. M. Gamba and S. H. Tharkabhushanam. Spectral-Lagrangian methods for collisional models of non-equilibrium statistical states. *J. Comput. Phys.*, 228(6):2012–2036, Apr. 2009.
- [31] I. M. Gamba and S. H. Tharkabhushanam. Shock and boundary structure formation by spectral-Lagrangian methods for the inhomogeneous Boltzmann transport equation. *J. Comput. Math.*, 28(4):430–460, 2010.
- [32] Y. Güçlü and W. N. G. Hitchon. A high order cell-centered semi-Lagrangian scheme for multi-dimensional kinetic simulations of neutral gas flows. *J. Comput. Phys.*, 231(8):3289–3316, 2012.
- [33] J. Haack and I. M. Gamba. High performance computing with a conservative spectral boltzmann solver. *28th International Symposium on Rarefied Gas Dynamics 2012*, 1501:334–341, 2012.
- [34] E. A. Malkov and M. S. Ivanov. Parallelization of algorithms for solving the boltzmann equation for gpu-based computations. *AIP Conference Proceedings*, 1333(1):946–951, 2011.
- [35] L. Mieussens. Discrete velocity model and implicit scheme for the BGK equation of rarefied gas dynamics. *Mathematical Models and Methods in Applied Sciences*, 10(08):1121–1149, 2000.
- [36] C. Mouhot and L. Pareschi. Fast algorithms for computing the Boltzmann collision operator. *Math. Comp.*, 75(256):1833–1852 (electronic), 2006.
- [37] K. Nanbu. Direct simulation scheme derived from the boltzmann equation. i. mono-component gases. *Journal of the Physical Society of Japan*, 49(5):2042–2049, 1980.
- [38] A. Palczewski and J. Schneider. Existence, stability, and convergence of solutions of discrete velocity models to the boltzmann equation. *Journal of statistical physics*, 91(1-2):307–326, 1998.
- [39] L. Pareschi and B. Perthame. A fourier spectral method for homogeneous Boltzmann equations. *Transport Theory Statist. Phys.*, 25(3):369–382, 1996.
- [40] L. Pareschi and G. Russo. Numerical solution of the Boltzmann equation I: Spectrally accurate approximation of the collision operator. *SIAM J. Numer. Anal.*, 37(4):1217–1245, 2000.
- [41] L. Pareschi, G. Toscani, and C. Villani. Spectral methods for the non cut-off Boltzmann equation and numerical grazing collision limit. *Numer. Math.*, 93(3):527–548, 2003.

- [42] M. Shoucri and G. Knorr. Numerical integration of the Vlasov equation. *J. Computational Phys.*, 14(1):84–92, 1974.
- [43] V. Titarev. Efficient deterministic modelling of three-dimensional rarefied gas flows. *Communications in Computational Physics*, 12(01):162–192, 2012.
- [44] V. Titarev, M. Dumbser, and S. Utyuzhnikov. Construction and comparison of parallel implicit kinetic solvers in three spatial dimensions. *Journal of Computational Physics*, 256:17–33, 2014.
- [45] E. F. Toro. *Riemann solvers and numerical methods for fluid dynamics: a practical introduction*. Springer Science & Business Media, 2013.
- [46] L. Wu, H. Liu, Y. Zhang, and J. M. Reese. Influence of intermolecular potentials on rarefied gas flows: Fast spectral solutions of the Boltzmann equation. *Physics of Fluids (1994-present)*, 27(8):082002, 2015.
- [47] L. Wu, C. White, T. J. Scanlon, J. M. Reese, and Y. Zhang. Deterministic numerical solutions of the Boltzmann equation using the fast spectral method. *Journal of Computational Physics*, 250:27–52, 2013.
- [48] L. Wu, C. White, T. J. Scanlon, J. M. Reese, and Y. Zhang. A kinetic model of the Boltzmann equation for non-vibrating polyatomic gases. *Journal of Fluid Mechanics*, 763:24–50, 2015.
- [49] L. Wu, J. Zhang, J. M. Reese, and Y. Zhang. A fast spectral method for the Boltzmann equation for monatomic gas mixtures. *Journal of Computational Physics*, 298:602–621, 2015.